Toward wall-modeled LES of particle-laden flows: Analysis of turbophoresis and inter-particle collisions in a turbulent channel flow

By P. L. Johnson

1. Motivation and objectives

Turbophoresis is the well-known tendency of inertial particles in turbulent fluid flows to drift down gradients of turbulence intensity (Caporaloni *et al.* 1975; Reeks 1983). In wall-bounded flows, the satisfaction of no-slip, no-penetration conditions for the fluid phase means that the turbulence intensities in the viscous sublayer are severely diminished compared to the rest of the flow. These two effects together lead to the tendency of particles to preferentially accumulate in the viscous sublayer (Marchioli & Soldati 2002; Sikovsky 2014). Even at relatively low volume fractions such as 10^{-5}, the local volume fraction in the viscous sublayer can be much higher. This effect, in combination with the strong mean shear, brings inter-particle collisional effects into play at far lower bulk volume fractions than typical (Elgobashi 1994).

Direct numerical simulations (DNS) of turbulent wall-bounded flows are possible at low Reynolds numbers, but the cost increases very quickly with Reynolds number. As a result, DNS is prohibitively expensive for high Reynolds number engineering flows. Large-eddy simulations (LES) have enjoyed a good deal of success and popularity in recent decades, but the strict near-wall grid requirements of wall-resolved LES still lead to sharp cost increases with Reynolds number (Chapman 1979; Choi & Moin 2012). Instead, various other more affordable simulation approaches have been invented for treating wall-bounded turbulent flows, such as detached-eddy simulations (DES) (Spalart 2009) and wall-modeled LES (Bose & Park 2018). These techniques save on computational cost by leaving out the resolution needed to capture near-wall eddies, although these eddies may be vital for the accurate simulation of turbophoresis and preferential accumulation of particles near the wall (Marchioli & Soldati 2002).

Although significant attention has been paid in recent years to enriching wall-resolved LES (WRLES) for particle-laden flows (Kuerten 2016; Marchioli 2017), the challenge of particle-laden wall-modeled LES (WMLES) is more difficult and more relevant for high Reynolds number flows. This report aims to clarify the physical mechanisms related to near-wall particle concentration, with an eye toward WMLES. In particular, it is important to understand the level of detail needed in recreating fluid velocities seen by particles within one grid spacing of the boundary in WMLES. Of course, such an understanding must encompass different regimes of inertial particle behaviors, including variations with Stokes number and volume fraction effects, among others. To this end, this report considers the consequences of the particle phase conservation equations in a turbulent channel flow in Section 2. In Section 3, point-particle DNS (PP-DNS) is used at $Re_\tau = 150$ to elucidate the qualitative observations from the momentum conservation equation. Conclusions are then drawn in Section 4.

2. Conservation equations for the particle phase

This section presents how conservation equations for the particle phase are systematically derived. Exact qualitative results follow directly from these conservation equations. For instance, the existence of a power-law singularity in the concentration profile at the wall in certain regimes follows directly from momentum conservation, and the exponent of this power-law can be formally bounded.

2.1. *Governing equations, flow geometry, and boundary conditions*

The fluid phase is described by a continuum with velocity $\mathbf{u}(\mathbf{x}, t)$ and pressure $p(\mathbf{x}, t)$ and evolves according to the incompressible Navier-Stokes equations,

$$\partial_t \mathbf{u} + (\mathbf{u} \cdot \nabla)\mathbf{u} = -\nabla(p/\rho_f) + \nu_f \nabla^2 \mathbf{u} + \mathbf{f}, \qquad \nabla \cdot \mathbf{u} = 0, \tag{2.1}$$

where $\mathbf{f}$ signifies forcing by particles. At the mass and volume fractions studied in this report, the two-way coupling represented by $\mathbf{f}$ is of secondary importance compared with particle-particle collisions and so is neglected in the numerical calculations presented here. The presence or absence of the two-way coupling does not change the conservation expressions derived below; however, it should be expected to quantitatively affect the drag force terms in these expressions when the mass fraction is high enough.

The particle phase is described by N_p discrete particles with center of mass $\mathbf{x}(t)$ and velocity $\mathbf{v}(t)$, evolving according to trajectory equations,

$$\dot{\mathbf{x}} = \mathbf{v} \qquad \dot{\mathbf{v}} = \mathbf{a}(\mathbf{x}, \mathbf{v}). \tag{2.2}$$

For small particles ($d_p < \eta$,δ_ν) at low Reynolds numbers, $Re_p = |\mathbf{u} - \mathbf{v}|d_p/\nu_f$, Stokes drag can be used, $\mathbf{a}_{St} = (\mathbf{u}(\mathbf{x}) - \mathbf{v})/\tau_p$, with relaxation time $\tau_p = \rho_p d_p^2/(18\mu_f)$ in the limit $\rho_p \gg \rho_f$. The Schiller-Naumann drag (Schiller & Naumann 1933; Balachandar & Eaton 2010), $\mathbf{a}_{SN} = \mathbf{a}_{St}(1 + 0.15Re_p^{0.687})$, gives a finite Reynolds number correction that is used for the simulations reported in this brief. The Stokes drag form is used at times within Section 2 to simplify expressions, but the same procedure also follows for Schiller-Naumann drag yielding finite Reynolds number correction terms, which are used to generate the plots in this report.

For studying the physics of wall-bounded flows in the simplest case possible, this report considers a turbulent channel flow. A negative unit pressure gradient is imposed in the streamwise (x) direction and no-slip, no-penetration conditions are imposed at the walls separated by a distance $2h$ in the y direction. Thus, the flow and particle statistics are homogeneous in the streamwise and spanwise (z) directions, with the only exception being the linearly decreasing mean pressure in the streamwise direction. A statistically stationary flow is considered.

2.2. *An evolution equation for the single-particle PDF*

Given statistical homogeneity in the x and z directions, the single-particle probability density function (PDF) of interest includes only wall-normal position and velocity,

$$f(y, v_y; t) = \langle \delta\left(y - \hat{y}(t)\right) \delta\left(v_y - \hat{v}_y(t)\right) \rangle, \tag{2.3}$$

where $\delta(x)$ is the Dirac delta function representing the fine-grained PDF. Here, the angled brackets, $\langle \cdot \rangle$, denote ensemble averaging. Assuming ergodic behavior, this is interchangeable with averaging in time and in the x-z plane, which is more convenient for obtaining the numerical results below.

To derive a dynamical equation for f, the individual particle dynamics of Eq. (2.2) are

projected in the wall-normal direction,

$$\dot{\hat{y}} = \hat{v}_y \qquad \dot{\hat{v}}_y = \hat{a}_y = \frac{u_y(\hat{\mathbf{x}}, t) - \hat{v}_y}{\tau_p}. \tag{2.4}$$

For simplicity, the following analysis assumes the Stokes drag formula, but generalization of the results to other drag forms is straightforward. In fact, corrections for Schiller-Naumann drag have been used for the numerical demonstrations below.

By differentiating Eq. (2.3) in time and substituting Eq. (2.4), one can obtain,

$$\partial_t f + \partial_y \left(v_y f\right) + \partial_{v_y} \left(\langle a_y | y, v_y \rangle f\right) = \dot{f}_{coll}, \tag{2.5}$$

where the conditional average $\langle a_y | y, v_y \rangle$ is shorthand for $\langle \hat{a}_y | \hat{y} = y, \hat{v}_y = v_y \rangle$, i.e., the average particle acceleration conditioned on wall-normal position and velocity. The right-hand side term $\dot{f}_{coll}$ refers to the effect of inter-particle collisions on redistributing particle velocities. Note that Eq. (2.5) is similar to that used by Sikovsky (2014), except in that work the fluid velocity seen by the particle (which contributes to the acceleration term) is modeled by a stochastic forcing term. Here, no stochastic modeling assumptions are made about the fluid flow seen by the particle, in order to understand the consequences of the exact conservation equations for the particle phase.

2.3. *The zeroth moment: particle mass conservation*

The normalized particle number density (concentration) is obtained at any y location by integrating f over all possible particle velocities,

$$C(y;t) = C_0 \int_{-\infty}^{\infty} f(y, v_y; t) dv_y, \tag{2.6}$$

where C_0 is the bulk particle concentration, $C_0 = \int_\Omega C(y) dy$. Integrating Eq. (2.5) over all velocities and multiplying by C_0, we obtain a conservation equation for the particle mass,

$$\partial_t C + \partial_y \left(\langle v_y | y \rangle C\right) = 0. \tag{2.7}$$

The collisional term vanishes because each collision individually conserves mass. For a stationary flow, $\partial_t C = 0$, which leads to $\langle v_y | y \rangle = 0$. This simply states that for statistical stationarity to be achieved, the net wall-normal flux of particles must vanish at all y locations.

2.4. *The first moment: particle momentum conservation*

The particle wall-normal momentum, which is the same as the particle mass flux in Eq. (2.7), is obtained as a first moment,

$$\langle v_y | y \rangle C(y;t) = C_0 \int_{-\infty}^{\infty} v_y f(y, v_y; t) dv_y. \tag{2.8}$$

Multiplying Eq. (2.5) by C_0 and v_y before integrating over all velocities yields the momentum conservation equation,

$$\partial_t \left(\langle v_y | y \rangle C\right) + \partial_y \left(\langle v_y^2 | y \rangle C\right) - \langle a_y | y \rangle C = 0. \tag{2.9}$$

The collisional term again vanishes because each collision conserves wall-normal momentum. The third term on the left, the acceleration term, is obtained using integration by

parts. At steady-state, $\partial_t \left(\langle v_y | y \rangle C \right) = 0$, and the momentum balance yields,

$$\frac{d}{dy} \left(\langle v_y^2 | y \rangle C \right) = \langle a_y | y \rangle C. \tag{2.10}$$

In this case, because $\langle v_y | y \rangle = 0$ from mass conservation, $\langle v_y^2 | y \rangle$ represents the particle wall-normal velocity variance as a function of distance from the wall. Note that the derivative in y on the left-hand side is now a total derivative since time-dependence is removed.

2.5. *Consequences of momentum conservation*

Using the product rule and assuming Stokes drag formula, the particle wall-normal momentum balance at steady-state, Eq. (2.10), may be rewritten as,

$$\langle v_y^2 | y \rangle \frac{dC}{dy} = \left(\frac{\langle u_y | y \rangle}{\tau_p} - \frac{d \langle v_y^2 | y \rangle}{dy} \right) C. \tag{2.11}$$

From this form, two mechanisms may be deduced for generating non-uniform particle concentrations. The second term on the right side is the turbophoresis pseudo-force, which creates the migration of particles from down gradients in wall-normal velocity variance. In a wall-bounded flow where no-slip, no-penetration boundary conditions are enforced on the fluid phase, the tendency of the particles to relax toward fluid velocities will give lower $\langle v_y^2 | y \rangle$ near the wall, leading to the well-known observation of increased particle concentrations in the viscous and buffer layers.

The first term on the right side of Eq. (2.11) represents the average wall-normal fluid velocity seen by particles at a given height. (Notice that the $\langle v_y | y \rangle$ contribution from Stokes drag vanishes due to mass conservation.) For particles which randomly sample the flow in an unbiased way, this term vanishes. However, it is known that heavy particles tend to accumulate in low-speed streaks associated with ejection events (Rashidi *et al.* 1990; Eaton & Fessler 1994; Marchioli & Soldati 2002). Indeed, as shown by the numerical results below, $\langle u_y | y \rangle > 0$ near the wall as particles sample ejection events more often than sweeps. As a result, this biased sampling term leads to a net drag force on particles away from the wall, opposing the turbophoresis force. Note that the analysis of Guha (1997, 2008) has omitted the biased sampling term, but for low Stokes numbers, this term provides significant opposition to turbophoresis.

At higher Stokes numbers, the τ_p in the denominator shows that the biased sampling force may be expected to diminish and become negligible compared to turbophoresis. It should be noted that the prediction of the turbophoresis force may not require detailed knowledge of particle interactions with turbulent coherent structures since it only relies on the gradient of particle wall-normal velocity variance. However, the dynamics of turbulent coherent structures plays a direct, unmistakable role in establishing the sampling bias term. One objective of the numerical demonstrations below is to quantify at what Stokes number one may safely neglect the biased sampling term in Eq. (2.11), and hence neglect the details of coherent structures.

2.5.1. *Phoresis integrals*

Equation (2.11) has the formal solution,

$$C(y) = \mathcal{N} \exp \underbrace{\left(\frac{1}{\tau_p} \int^y \frac{\langle u_y|\eta\rangle}{\langle v_y^2|\eta\rangle} d\eta \right.}_{\text{biased sampling}} \underbrace{\left. - \int^y \frac{d \ln\langle v_y^2|\eta\rangle}{d\eta} d\eta \right)}_{\text{turbophoresis}}, \tag{2.12}$$

where $\mathcal{N}$ is an integration constant that depends on the (unspecified) lower bound of the integrals. This form is useful for defining two phoresis integrals as underscored in the equation. The first phoresis integral,

$$I_{bias} = \frac{1}{\tau_p} \int_0^y \frac{\langle u_y|\eta\rangle}{\langle v_y^2|\eta\rangle} d\eta, \tag{2.13}$$

can be computed from numerical simulations to directly quantify the impact of biased sampling on the resulting concentration profile. Meanwhile, the second phoresis integral,

$$I_{turb} = \int_0^y \frac{d \ln\langle v_y^2|\eta\rangle}{d\eta} d\eta, \tag{2.14}$$

quantifies the influence of turbophoresis on the final concentration profile. In these two definitions, the wall location ($y = 0$) is used for the lower bound. These two definitions give a simple way to make an apples-to-apples comparison of how biased sampling and turbophoresis affect the concentration profile (and when one effect may be neglected).

2.5.2. *Large Stokes number particles*

Seeing that the turbophoresis integral, Eq. (2.14), may be formally integrated, then Eq. (2.12) may also be written as

$$C(y) = \frac{\mathcal{N}}{\langle v_y^2|y\rangle} \exp\left(\frac{1}{\tau_p} \int^y \frac{\langle u_y|\eta\rangle}{\langle v_y^2|\eta\rangle} d\eta \right). \tag{2.15}$$

This form emphasizes that, at large Stokes numbers when the biased sampling becomes negligible, the concentration profile become inversely proportional to the wall-normal particle velocity variance. From a modeling perspective, this means that predicting concentration profiles for high Stokes number particles,

$$C(y) \approx \frac{\mathcal{N}}{\langle v_y^2|y\rangle}, \tag{2.16}$$

requires only an accurate representation of wall-normal fluctuation magnitudes. The spatio-temporal details of interactions between particles and near-wall coherent structures becomes unimportant in this limit, simplifying the modeling task.

2.5.3. *The tracer particle limit*

In the limit $\tau_p \to 0$, the particle velocity may be written as (Maxey 1987)

$$v_y = u_y - \tau_p \frac{Du_y}{Dt} + \mathcal{O}(\tau_p^2). \tag{2.17}$$

This means that the biased sampling force becomes

$$\lim_{\tau_p \to 0} \frac{\langle u_y|y\rangle}{\tau_p} = \left\langle \frac{Du_y}{Dt} \right\rangle = -\frac{1}{\rho_f} \frac{\partial\langle p\rangle}{\partial y}. \tag{2.18}$$

Note that the viscous force, $\nu_f \nabla^2 \langle u_y \rangle$, vanishes because $\langle u_y \rangle = 0$ at steady-state in the limit $\tau_p \to 0$. At $\tau_p = 0$, the average over the particle ensemble becomes the same as the fluid ensemble average, the concentration profile becomes flat (incompressibility), and the wall-normal Reynolds-averaged Navier-Stokes equation (RANS) is obtained from Eq. (2.11),

$$0 = -\frac{\partial \langle p \rangle}{\partial y} + \frac{d \left\langle u_y^2 \right\rangle}{dy}, \tag{2.19}$$

as in, for example, equation (5.2.2) of Tennekes & Lumley (1972). This convergence of the $St \to 0$ limit of the biased sampling to the pressure gradient was previously pointed out in passing by Bragg & Collins (2014) during a discussion of the analogy between preferential concentration in homogeneous turbulence and turbophoresis in wall-bounded turbulence.

2.5.4. *Particles near the wall*

The existence of a power-law concentration profile in the viscous sublayer can be derived exactly in the low Stokes number limit. The reasons a power-law is observed at higher Stokes numbers stem also from this analysis and are discussed below. Consider Eq. (2.17) in the limit $y \to 0$, where a Taylor expansion of the fluid velocity field prevails,

$$\begin{aligned} u_x(x,y,z,t) &= A_x(x,z,t)y + \mathcal{O}(y^2), \\ u_y(x,y,z,t) &= A_y(x,z,t)y^2 + \mathcal{O}(y^3), \\ u_z(x,y,z,t) &= A_z(x,z,t)y + \mathcal{O}(y^2). \end{aligned} \tag{2.20}$$

Note that the linear term $\sim y$ for the wall-normal fluid velocity is exactly zero due to the divergence-free condition for incompressible flows (Kim *et al.* 1987; Pope 2000). Substituting Eq. (2.20) into Eq. (2.17), i.e.,

$$v_y = u_y - \tau_p \left(\partial_t u_y + u_x \partial_x u_y + u_y \partial_y u_y + u_z \partial_z u_y \right) + \mathcal{O}(\tau_p^2),$$

one obtains

$$v_y = A_y y^2 - \tau_p \left(y^2 \partial_t A_y + y^3 A_x \partial_x A_y + y^4 A_y \partial_y A_y + y^3 A_z \partial_z A_y \right) + \mathcal{O}(\tau_p^2, y^3). \tag{2.21}$$

From this expression, we can evaluate

$$\langle v_y^2 | y \rangle = \underbrace{\langle A_y^2 \rangle}_{\alpha} y^4 + \mathcal{O}(\tau_p, y^5), \tag{2.22}$$

where we have used $\langle \partial_t A_y \rangle = 0$ and $\langle A_y \partial_t A_y \rangle = 0$ owing to stationarity. Furthermore, we can evaluate the biased sampling term,

$$\frac{\langle u_y | y \rangle}{\tau_p} = \frac{\langle (u_y - v_y) | y \rangle}{\tau_p} = \underbrace{\langle A_x \partial_x A_y + A_z \partial_z A_y \rangle}_{\beta} y^3 + \mathcal{O}(\tau_p, y^4). \tag{2.23}$$

Together, Eqs. (2.22) and (2.23) yield

$$\begin{aligned} \langle v_y^2 | y \rangle &\approx \alpha y^4, \\ \langle u_y | y \rangle &\approx \beta \tau_p y^3, \end{aligned} \tag{2.24}$$

with $\alpha > 0$ and $\beta > 0$ (observed bias toward ejection events). Although this has been derived specifically in the $\tau_p \to 0$ limit, the numerical results below show that this scaling is observed over a generous range of finite Stokes numbers. In fact, it is reasonable to expect that the scalings in Eq. (2.24) hold over a decent range of finite Stokes numbers because the particle ensemble averages are biased toward particles with larger residence

time in the near-wall region (trapped particles). Even at finite Stokes numbers, these particles with longer residence times by definition have more time to adjust to the local near-wall fluid scalings.

Substituting Eq. (2.24) into Eq. (2.15),

$$C(y) = \frac{\mathcal{N}}{\alpha y^4} \exp\left(\int^y \frac{\beta \eta^3}{\alpha \eta^4} d\eta\right) = \frac{\mathcal{N}}{\alpha} y^{\beta/\alpha - 4}. \tag{2.25}$$

At $\tau_p = 0$, it must be true that $\beta = 4\alpha$ according to Eq. (2.19). At large Stokes numbers, it must be that $\beta \to 0$ for $\langle u_y | y \rangle$ to remain finite. At finite Stokes numbers, provided the near-wall scalings given by Eq. (2.24) hold, $0 < \beta < 4\alpha$, then the concentration profile in the viscous sublayer has the form

$$C(y) \sim y^{-\gamma}, \tag{2.26}$$

with $0 < \gamma < 4$. Thus, from the momentum balance, reasonable assumptions lead to an expected near-wall power-law in the concentration profile, with power-law exponent bounded by $\gamma < 4$, in agreement with previous stochastic models and observed DNS trends (Sikovsky 2014). As illustrated below, inter-particle collisions can interrupt this power-law behavior when the volume fraction is large enough by energizing near-wall particles away from the $\langle v_y^2 | y \rangle$ scaling in Eq. (2.24).

2.6. *Higher-order moments and consequences*

Following the same procedure for higher-order moments,

$$\langle v_y^n | y \rangle C(y;t) = C_0 \int_{-\infty}^{\infty} v_y^n f(y, v_y; t) dv_y. \tag{2.27}$$

After explicitly neglecting collisional effects, the n^{th} moment of Eq. (2.5) gives

$$\partial_t(\langle v_y^n | y \rangle C) + \partial_{v_y}(\langle v_y^{n+1} | y \rangle C) - n \langle a_y v_y^{n-1} | y \rangle C = 0. \tag{2.28}$$

At steady-state for particles experiencing Stokes drag,

$$\langle v_y^{n+1} | y \rangle \frac{dC}{dy} = \left(\frac{n}{\tau_p} \langle (u_y - v_y) v_y^{n-1} | y \rangle - \frac{d\langle v_y^{n+1} | y \rangle}{dy} \right) C, \tag{2.29}$$

which has the formal solution

$$C(y) = \frac{\mathcal{N}'}{\langle v_y^{n+1} | y \rangle} \exp\left(\frac{n}{\tau_p} \int^y \frac{\langle (u_y - v_y) v_y^{n-1} | \eta \rangle}{\langle v_y^{n+1} | \eta \rangle} d\eta \right). \tag{2.30}$$

Dividing this expression with Eq. (2.15) raised to the $(n+1)/2$ power and rearranging yields,

$$\frac{\langle v_y^m \rangle}{\langle v_y^2 \rangle^{m/2}} = \mathcal{N}'' C(y)^{m/2-1} \exp\left(\frac{m-1}{\tau_p} \int^y \frac{\langle (u_y - v_y) v_y^{m-2} | \eta \rangle}{\langle v_y^m | \eta \rangle} d\eta - \frac{m}{2\tau_p} \int^y \frac{\langle u_y | \eta \rangle}{\langle v_y^2 | \eta \rangle} d\eta \right), \tag{2.31}$$

where $m = n + 1$ has been substituted. Therefore, when the concentration profile has a power-law given by Eq. (2.26), and similar scaling arguments to those in Section 2.5.4 hold, this expression gives a power-law for the skewness, flatness, and other higher-order hyper-flatness values. In particular,

$$\frac{\langle v_y^m \rangle}{\langle v_y^2 \rangle^{m/2}} \sim y^{-\gamma(m/2-1)+\delta}, \tag{2.32}$$

where the δ comes from the exponential term in Eq. (2.31). Note that as τ_p increases, this exponential term becomes small, leading to $\delta \to 0$ as $St^+ \to \infty$. This limit is in agreement with the stochastic model of Sikovsky (2014), though that model apparently misses the correction term for smaller Stokes numbers. This is further apparent in the fact that their results for flatness, $m = 4$, give better agreement at $St^+ = 25$ than at $St^+ = 5$ (the author omits $St^+ = 1$ results claiming that the profiles had not yet fully developed, but it is more likely that the exponential correction term is the culprit).

3. Simulations with and without collisions

3.1. *Numerical details*

The continuum equations for the fluid, Eq. (2.1), are discretized on a staggered Cartesian grid, and second-order central differencing is employed. Trilinear interpolation is used to compute the flow quantities (e.g., velocity) at the particle location for the drag law, Eq. (2.2). A fractional step method for time advancement for the fluid and particles is done with Huen's second-order method (RK2). The grid resolution used in the homogeneous directions is $\Delta x^+ \approx 11$, $\Delta z^+ \approx 7$. The grid is stretched in the wall-normal direction using a hyperbolic tangent to yield $\Delta y^+_{min} \approx 0.5$ for the first grid point at the wall (wall-parallel velocities at $y^+ \approx 0.25$) and $\Delta y^+_{max} \approx 7$ in the center of the channel. This resolution might be considered slightly under-resolved for a true DNS. However, sensitivity of the particle concentration profile to further refinement was explored and found to be small, so this grid resolution may be considered sufficient for the present purposes while keeping computational costs low. The particles are initialized with a uniform random distribution, and the simulation proceeds until the particles obtain a stationary distribution before statistics are computed.

The computational domain is periodic in x and z with domain size large enough to prevent significant effects from false periodicity ($L_x = 4\pi h$, $L_y = 2h$, $L_z = 2\pi h$). The imposed pressure gradient is simulated by a uniform body force to reach a friction Reynolds number of $Re_* = u_* h/\nu = 150$, which is sufficiently turbulent to study the main features of particles in wall-bounded flows without incurring high computational costs. The relative influence of particle inertial is captured by the friction Stokes number, $St^+ = \tau_p/\tau_* = u_*^2 \tau_p/\nu$, where $u_*^2 = -h(dp/dx)/\nu_f$ is the friction velocity. The other dimensionless parameter considered in this report is the volume fraction, $\Phi_V = \pi d_p^3 N_p/(6 L_x L_y L_z)$, where N_p is the total number of particles in the domain. Results at $Re_\tau = 600$ (not shown) have indicated that the results discussed in this brief are fairly invariant with Re_τ.

3.2. *Without inter-particle collisions*

Figure 1 shows the main results for the statistics of particle ensembles without inter-particle collisions at $Re_\tau = 150$ for a range of $0 \leq St^+ \leq 512$, using $d_p^+ = 0.5$ and changing $144 \leq \rho_p \leq 36,864$ to change St^+. These ensembles represent the limit of $\Phi_V \to 0$. As can be seen from Figure 1(a), in the absence of inter-particle collisions, the concentration near the wall can reach hundreds of times larger than the mean concentration level. This effect is driven by turbophoresis, $C \sim \langle v_y^2 | y \rangle^{-1}$. Note that the $St^+ = 0$ tracer particles have a flat distribution with slight interpolation and time discretization errors leading to an almost imperceptibly reduced concentration in the viscous sublayer.

The particle root-mean-square fluctuations, $\sqrt{\langle v_y^2 | y \rangle}$, shown in Figure 1(b), reveal that the asymptotic $v_y \sim y^2$ behavior near the wall persists even up to relatively high St^+.

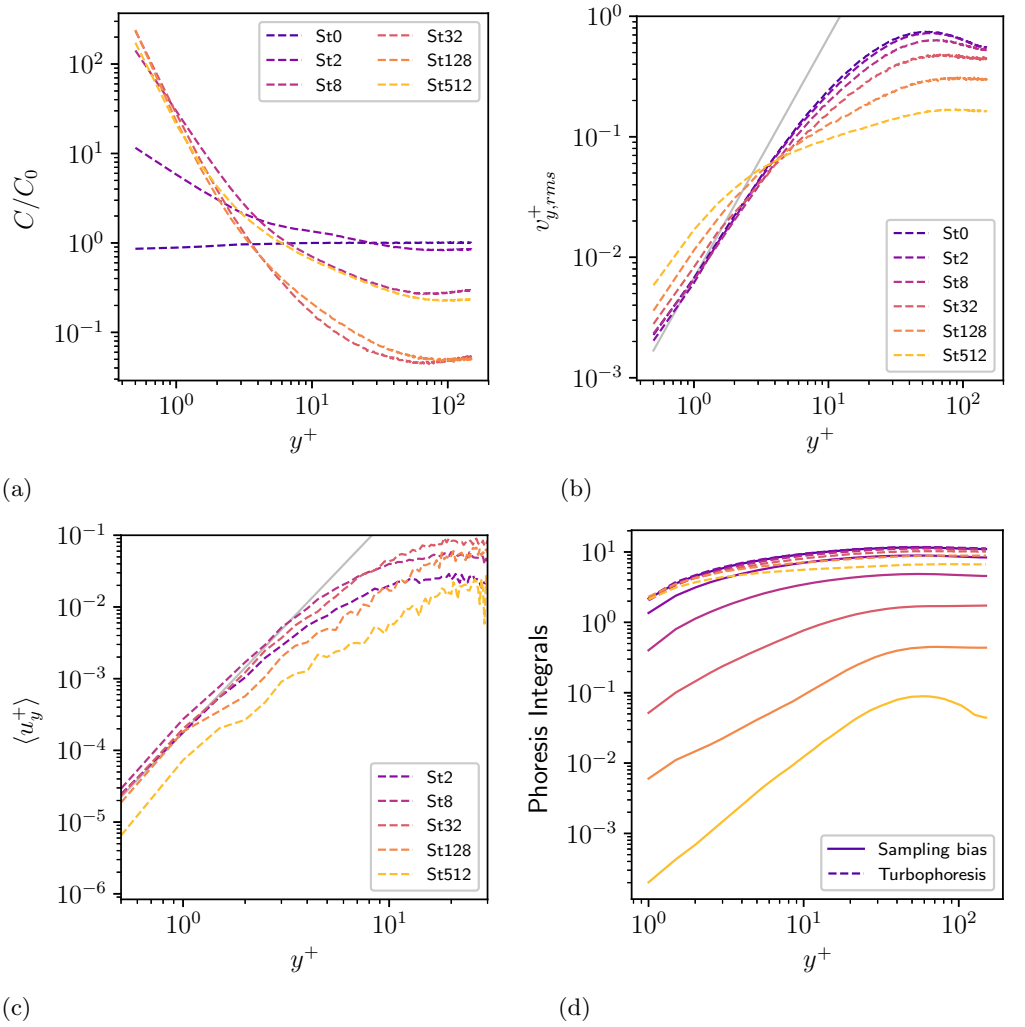

FIGURE 1. Particles statistics from turbulent channel flow at $Re_\tau = 150$ in the zero volume fraction limit (no inter-particle collisions) at various Stokes numbers: (a) concentration profiles; (b) root-mean-square wall-normal particle velocity, where the continuous gray curve indicates $v_y \sim y^2$ asymptotic behavior near the wall; (c) sampling bias $\langle u_y|y \rangle$ for the particle ensembles with continuous gray line indicating $\sim y^3$ behavior near the wall; (d) sampling bias and turbophoresis integrals, see Eqs. (2.13) and (2.14).

Meanwhile, Figure 1(c) shows the sampling bias term $\langle u_y|y \rangle$, demonstrating that the $\sim y^3$ behavior of that terms also extends to relatively large values of St^+. Taken together, these two figures justify the scaling behavior, Eq. (2.24), used in Section 2.5.4 well beyond the low Stokes number regime of Maxey (1987). Further investigation into this observation (not shown) elucidates that this happens because particle statistics near the wall are dominated by trapped particles with long enough residence times to adjust to viscous sublayer fluid fluctuations despite nominally large St^+.

The resulting phoresis integrals, Eqs. (2.13) and (2.14), are shown in Figure 1(d). The integrals are both positive in all cases and are computed using a trapezoidal rule

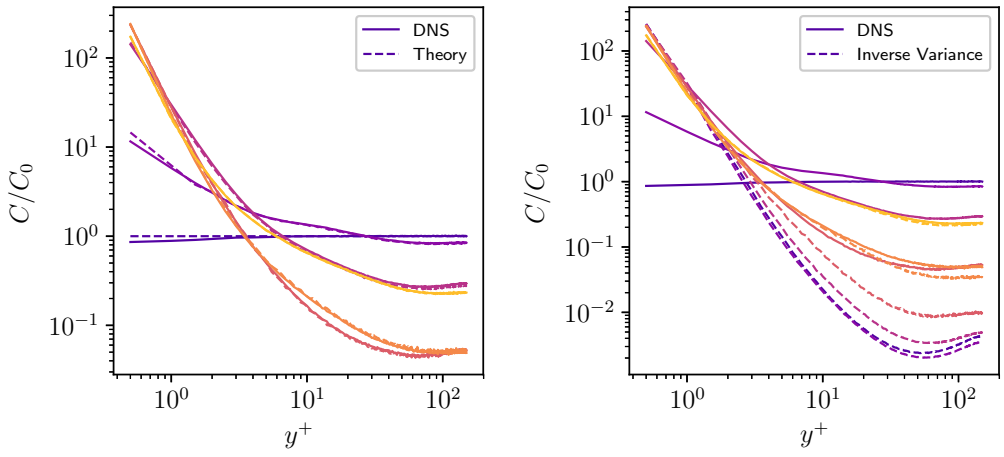

(a) (b)

FIGURE 2. For $\Phi_V = 0$, the comparison of left (continuous lines) and right sides (dashed lines) of (a) Eq. (2.12) and (b) Eq. (2.16). Colors indicate St^+ following the legend in Figure 1.

integration. The exponential of their difference is the concentration profile, as verified in Figure 2. At $St^+ = 2$, the sampling bias term mostly cancels the turbophoresis term. As the Stokes number is increased, however, the sampling bias term decreases sharply, leading to the more extreme near-wall enhancements of the concentration profile seen in Figure 1. At a large enough Stokes number, say $St^+ \geq 128$, the sampling bias integral is negligible compared to the turbophoresis integral, showing that the concentration profile is simply inversely proportional to the particle velocity variance as in Eq. (2.16). It should be noted, however, that for these high Stokes numbers, the particle wall-normal velocity variance deviates significantly from that of the fluid at any given distance from the wall. Therefore, it is still non-trivial that a WMLES designed to reproduce fluid velocity variances in the near-wall region would necessarily produce accurate particle velocity variances and concentration profiles, even in the high Stokes number limit.

For completeness, Eq. (2.12) for the concentration profile is directly verified by comparing left and right sides in Figure 2(a). In Figure 2(b), the same comparison is done using Eq. (2.16) instead, i.e., neglecting the sampling bias effect. This further emphasizes that for $St^+ \geq 128$, the details of the interactions between particles and turbulent structures near the wall are not important. Instead, the concentration profile can be predicted simply by the inverse of the particle wall-normal velocity variance.

3.3. *With inter-particle collisions*

Figure 3 shows the same statistics for particle ensembles including inter-particle collisions. For brevity, only $St^+ = 32$ is considered, although the main observations made here apply to other Stokes numbers as well. The most striking observation to be made from Figure 3(a) is that the enhanced concentration near the wall due to turbophoresis is suppressed by the effect of inter-particle collisions even at seemingly innocuous bulk volume fractions. With volume fraction increased to $\Phi_V = 10^{-4}$, the peak concentration profile at the wall is less than five times the bulk concentration. Collisional effects on the concentration profile are seen even for volume fractions as low as $\Phi_V = 10^{-6}$.

The main cause of this change is demonstrated in Figure 3(b), where the particle wall-

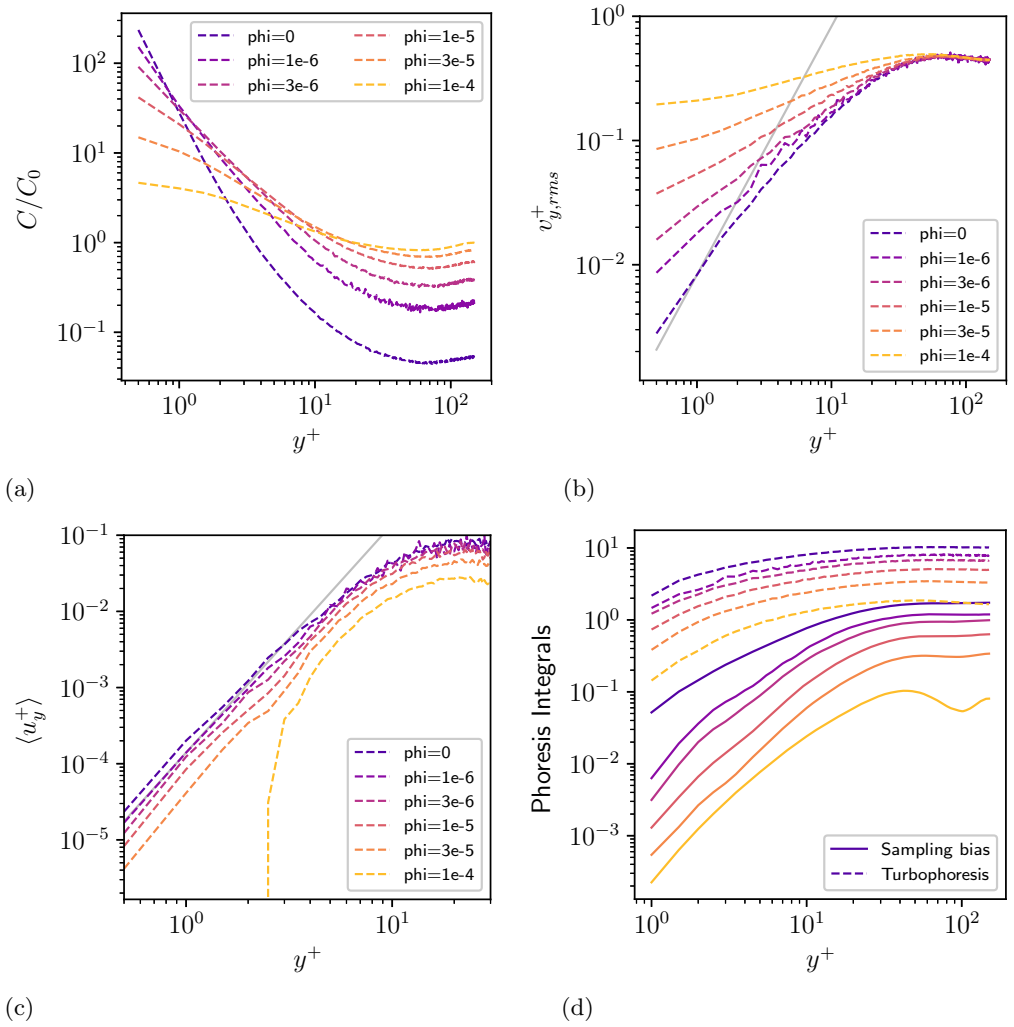

FIGURE 3. Statistics for $St^+ = 32$ particles in a turbulent channel flow at $Re_\tau = 150$ at various volume fractions. Descriptions of subfigures are the same as in Figure 1.

normal fluctuations near the wall increase dramatically above the fluid fluctuation levels as volume fraction is increased. The increased levels of fluctuation can be attributed to a more ballistic behavior of particles as they collide more frequently and redistribute streamwise fluctuations into wall-normal fluctuations. This also impacts the sampling bias, as shown in Figure 3(c). However, for $St^+ = 32$ shown here, the turbophoresis integral dominates over the sampling bias integral, Figure 3(d), showing that the spatio-temporal details of interactions with near-wall turbulent structures have little effect on the concentration profile. The increased fluctuations near the wall, far in excess of local fluid fluctuation levels, break the scaling behaviors of Eq. (2.24), and this leads to the near-wall power-law in concentration. In fact, Figure 3 shows that the concentration profiles for higher volume fraction cases no longer display convincing power-laws near the wall.

The verification of Eq. (2.12) is included in Figure 4 for the cases with inter-particle

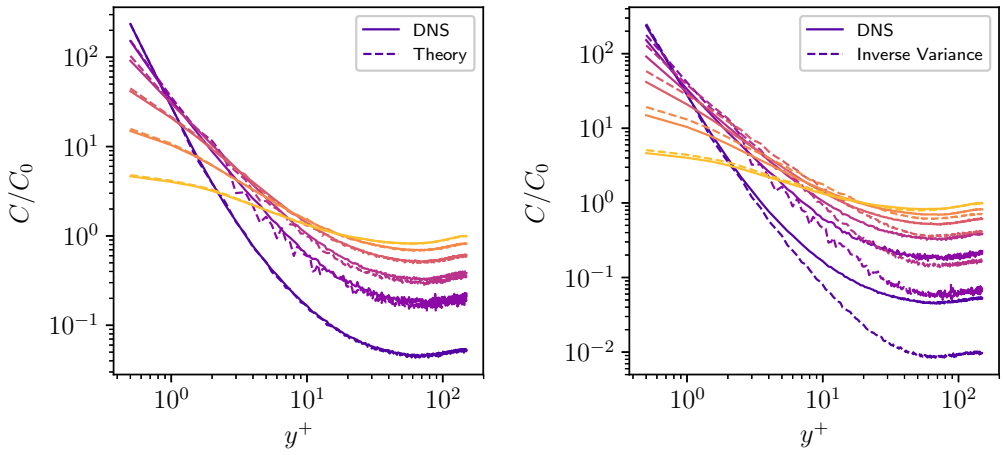

(a) (b)

FIGURE 4. For $St^+ = 32$, the comparison of left (continuous lines) and right sides (dashed lines) of (a) Eq. (2.12) and (b) Eq. (2.16). Colors indicate Φ_V following the legend in Figure 3.

collisions. The conservation of momentum by particle collisions ensures that the $\dot{f}_{coll}$ term does not contribute, and Eq. (2.15) accurately describes the concentration profiles in both cases. For $St^+ = 32$, as the volume fraction increases, the sampling bias integral decreases more quickly than the turbophoresis integral, meaning that the higher volume fraction cases have concentration profiles very close to the inverse of their wall-normal particle velocity variance profiles.

4. Conclusions

The work discussed in this report demonstrates that many of the features known about particle concentration profiles in wall-bounded turbulence can be found simply by considering exact conservation equations for the particle phase, without any stochastic modeling assumptions. In particular, the momentum balance at steady-state can be formally solved for the non-uniform concentration profile in terms of turbophoresis and sampling bias contributions. Although the turbophoresis term has been known and explored in many previous theoretical studies (Caporaloni *et al.* 1975; Reeks 1983; Guha 1997), the sampling bias term has not received the same attention. In some cases, it is (presumably) absorbed into a stochastic model (Sikovsky 2014) and in other cases it has been simply left out (Guha 1997, 2008)! While previous numerical studies have focused on connecting turbophoresis with near-wall coherent structures (Marchioli & Soldati 2002; Guingo & Minier 2008; Jin *et al.* 2015) the analysis here highlights the biased sampling term through which the influence of coherent structures more directly enters the particle equations. In particular, the sampling bias term is important at low Stokes numbers and enforces a uniform concentration in the zero Stokes limit. Furthermore, it follows from this analysis that the sampling bias becomes unimportant at high Stokes numbers, leading to a concentration profile that is inversely proportional to the particle wall-normal velocity variance. This has an important consequence for WMLES, which in this regime only requires accurate fluctuation intensity profiles and likely need

not recover the spatio-temporal details of interactions between particles and near-wall turbulent structures.

In the limit approaching the wall (i.e., within the viscous sublayer), the emergence of a power-law in the concentration profile is a direct consequence of momentum conservation, without any ad-hoc modeling assumptions needed. This observation brings clarity as to why concentration profiles have been observed to follow quite convincing power-law behaviors near the wall over a range of Stokes numbers. In fact, the scalings necessary for the existence of this power-law are theoretically justifiable only in the low Stokes number limit but can hold even to quite high Stokes numbers due to the trapping of slower-moving particles for long residence times near the wall. Particle-particle collisions, however, break the scalings even at quite low bulk volume fractions owing to the increased fluctuation levels near the wall that deviate from the asymptotic behavior of fluid fluctuations. When the concentration profile has a power-law, a related power-law exists for the skewness, flatness, and higher-order normalized moments, as shown from the exact conservation equations for higher-order velocity moments. Thus, the key results of Sikovsky (2014), there derived using a stochastic model for the fluid velocity, are derived and even improved upon here with no modeling assumptions.

Acknowledgments

This investigation was funded by the Advanced Simulation and Computing program of the US Department of Energy's National Nuclear Security Administration via the PSAAP-II Center at Stanford, Grant No. DE-NA0002373. Over the course of working on this project, I was motivated by and benefited from discussions with Parviz Moin, Javier Urzay, Maxime Bassenne, Mahdi Esmaily (Cornell University), Marco Giometto (Columbia University), and Xiang Yang (Penn State University).

REFERENCES

Balachandar, S. & Eaton, J. K. 2010 Turbulent dispersed multiphase flow. *Annu. Rev. Fluid Mech.* **42**, 111–133.

Bose, S. T. & Park G. I. 2018 Wall-modeled LES for complex turbulent flows. *Annu. Rev. Fluid Mech.* **50**, 535-561.

Bragg, A. D. & Collins, L. R. 2014 New insights from comparing statistical theories for inertial particles in turbulence: I. Spatial distribution of particles. *New J. Phys.* **16**, 055013.

Caporaloni, M., Tampieri, F., Trombetti, F. & Vittori, O. 1975 Transfer of particles in nonisotropic air turbulence. *J. Atmos. Sci.* **32**, 565–568.

Chapman, D. R. 1979 Computational aerodynamics development and outlook. *AIAA J.* **17**, 1293–1313.

Choi, H. & Moin, P. 2012 Grid-point requirements for large eddy simulation: Chapman's estimates revisited. *Phys. Fluids* **24**, 011702.

Eaton, J. K. & Fessler, J. R. 1994 Preferential concentration of particles by turbulence. *Int. J. Multiphase Flow* **20**, 169–209.

Elgobashi, S. 1994 On predicting particle-laden turbulent flows. *Appl. Sci. Res.* **52**, 309–329.

Guha, A. 1997 A unified Eulerian theory of turbulent deposition to smooth and rough surfaces. *J. Aerosol Sci.* **28**, 1517–1537.

Guha, A. 2008 Transport and deposition of particles in turbulent and laminar flow. *Annu. Rev. Fluid Mech.* **40**, 311–341.

Guingo, M. & Minier, J.-P. 2008 A stochastic model of coherent structures for particle deposition in turbulent flows. *Phys. Fluids* **20**, 053303.

Jin, C., Potts, I. & Reeks, M. W. 2015 A simple stochastic quadrant model for the transport and deposition of particles in turbulent boundary layers. *Phys. Fluids* **27**, 053305.

Kim, J., Moin, P. & Moser, R. 1987 Turbulence statistics in fully developed channel flow at low Reynolds number. *J. Fluid Mech.* **177**, 133–166.

Kuerten, J. G. M. 2016 Point-particle DNS and LES of particle-laden turbulent flow – a state-of-the-art review. *Flow Turbul. Combust.* **97**, 689–713.

Marchioli, C. 2017 Large-eddy simulation of turbulent dispersed flows: a review of modelling approaches. *Acta Mech.* **228**, 741–771.

Marchioli, C. & Soldati, A. 2002 Mechanisms for particle transfer and segregation in a turbulent boundary layer. *J. Fluid Mech.* **468**, 283–315.

Maxey, M. R. 1987 The gravitational settling of aerosol particles in homogeneous turbulence and random flow fields. *J. Fluid Mech.* **174**, 441–465.

Pope, S. B. 2000 *Turbulent Flows*. Cambridge University Press.

Rashidi, M., Hetstroni, G. & Banerjee, S. 1990 Particle-turbulence interaction in a boundary layer. *Int. J. Multiphas. Flow* **16**, 935–949.

Reeks, M. W. 1983 The transport of discrete particles in inhomogeneous turbulence. *J. Aerosol Sci.* **14**, 729–739.

Schiller, L. & Naumann, A. Z. 1933 Uber die grundlegenden berechnungen bei der schwekraftaubereitung. *Z. Ver. Dtsch. Ing.* **77**, 318–320.

Sikovsky, D. P. 2014 Singularity of inertial particle concentration in the viscous sublayer of wall-bounded turbulent flows. *Flow Turbul. Combust.* **95**, 561–582 275–308.

Spalart, P. R. 2009 Detached-eddy simulation. *Annu. Rev. Fluid Mech.* **41**, 181–202.

Tennekes, H. & Lumley, J. L. 1972 *A First Course in Turbulence*. MIT Press.